BRAIN COMMUNICATIONS

Molecular neuroimaging in dominantly inherited versus sporadic early-onset Alzheimer's disease

Leonardo Iaccarino,[1],* Jorge J. Llibre-Guerra,[2,3],* Eric McDade,[2,3] Lauren Edwards,[1] Brian Gordon,[4] Tammie Benzinger,[4] Jason Hassenstab,[2,3] Joel H. Kramer,[1] Yan Li,[5] Bruce L. Miller,[1] Zachary Miller,[1] John C. Morris,[2,3] Nidhi Mundada,[1] Richard J. Perrin,[6] Howard J. Rosen,[1] David Soleimani-Meigooni,[1] Amelia Strom,[1] Elena Tsoy,[1] Guoqiao Wang,[5] Chengjie Xiong,[5] Ricardo Allegri,[7] Patricio Chrem,[7] Silvia Vazquez,[7] Sarah B. Berman,[8] Jasmeer Chhatwal,[9] Colin L. Masters,[10] Martin R. Farlow,[11] Mathias Jucker,[12] Johannes Levin,[13,14,15] Stephen Salloway,[16] Nick C. Fox,[17] Gregory S. Day,[18] Maria Luisa Gorno-Tempini,[1] Adam L. Boxer,[1] Renaud La Joie,[1] Randall Bateman[2,3],† and Gil D. Rabinovici[1,19],†

* These authors contributed equally to this work and share first authorship.
† These authors contributed equally to this work and share senior authorship.

Approximately 5% of Alzheimer's disease patients develop symptoms before age 65 (early-onset Alzheimer's disease), with either sporadic (sporadic early-onset Alzheimer's disease) or dominantly inherited (dominantly inherited Alzheimer's disease) presentations. Both sporadic early-onset Alzheimer's disease and dominantly inherited Alzheimer's disease are characterized by brain amyloid-β accumulation, tau tangles, hypometabolism and neurodegeneration, but differences in topography and magnitude of these pathological changes are not fully elucidated. In this study, we directly compared patterns of amyloid-β plaque deposition and glucose hypometabolism in sporadic early-onset Alzheimer's disease and dominantly inherited Alzheimer's disease individuals. Our analysis included 134 symptomatic sporadic early-onset Alzheimer's disease amyloid-Positron Emission Tomography (PET)-positive cases from the University of California, San Francisco, Alzheimer's Disease Research Center (mean ± SD age 59.7 ± 5.6 years), 89 symptomatic dominantly inherited Alzheimer's disease cases (age 45.8 ± 9.3 years) and 102 cognitively unimpaired non-mutation carriers from the Dominantly Inherited Alzheimer Network study (age 44.9 ± 9.2). Each group underwent clinical and cognitive examinations, ^{11}C-labelled Pittsburgh Compound B-PET and structural MRI. ^{18}F-Fluorodeoxyglucose-PET was also available for most participants. Positron Emission Tomography scans from both studies were uniformly processed to obtain a standardized uptake value ratio (PIB$_{50-70}$ cerebellar grey reference and FDG$_{30-60}$ pons reference) images. Statistical analyses included pairwise global and voxelwise group comparisons and group-independent component analyses. Analyses were performed also adjusting for covariates including age, sex, Mini-Mental State Examination, apolipoprotein ε4 status and average composite cortical of standardized uptake value ratio. Compared with dominantly inherited Alzheimer's disease, sporadic early-onset Alzheimer's disease participants were older at age of onset (mean ± SD, 54.8 ± 8.2 versus 41.9 ± 8.2, Cohen's $d = 1.91$), with more years of education (16.4 ± 2.8 versus 13.5 ± 3.2, $d = 1$) and more likely to be apolipoprotein ε4 carriers (54.6% ε4 versus 28.1%, Cramer's $V = 0.26$), but similar Mini-Mental State Examination (20.6 ± 6.1 versus 21.2 ± 7.4, $d = 0.08$). Sporadic early-onset Alzheimer's disease had higher global cortical Pittsburgh Compound B-PET binding (mean ± SD standardized uptake value ratio, 1.92 ± 0.29 versus 1.58 ± 0.44, $d = 0.96$) and greater global cortical ^{18}F-fluorodeoxyglucose-PET hypometabolism (mean ± SD standardized uptake value ratio, 1.32 ± 0.1 versus 1.39 ± 0.19, $d = 0.48$) compared with dominantly inherited Alzheimer's disease. Fully adjusted comparisons demonstrated relatively higher

Pittsburgh Compound B-PET standardized uptake value ratio in the medial occipital, thalami, basal ganglia and medial/dorsal frontal regions in dominantly inherited Alzheimer's disease versus sporadic early-onset Alzheimer's disease. Sporadic early-onset Alzheimer's disease showed relatively greater ^{18}F-fluorodeoxyglucose-PET hypometabolism in Alzheimer's disease signature temporoparietal regions and caudate nuclei, whereas dominantly inherited Alzheimer's disease showed relatively greater hypometabolism in frontal white matter and pericentral regions. Independent component analyses largely replicated these findings by highlighting common and unique Pittsburgh Compound B-PET and ^{18}F-fluorodeoxyglucose-PET binding patterns. In summary, our findings suggest both common and distinct patterns of amyloid and glucose hypometabolism in sporadic and dominantly inherited early-onset Alzheimer's disease.

1   Memory and Aging Center, Department of Neurology, Weill Institute for Neurosciences, University of California San Francisco, San Francisco, CA 94158, USA
2   The Dominantly Inherited Alzheimer Network (DIAN), St Louis, MO 63108, USA
3   Department of Neurology, Washington University in St Louis, St Louis, MO 63108, USA
4   Department of Radiology, Washington University in St Louis, St Louis, MO 63110, USA
5   Department of Biostatistics, Washington University in St Louis, St Louis, MO 63110, USA
6   Department of Pathology and Immunology, Washington University in St Louis, St Louis, MO 63110, USA
7   Department of Cognitive Neurology, Institute for Neurological Research Fleni, Buenos Aires 1428, Argentina
8   Department of Neurology, University of Pittsburgh, Pittsburgh, PA 15213, USA
9   Massachusetts General Hospital, Harvard Medical School, Boston, MA 02114, USA
10 Department of Neuroscience, Florey Institute, The University of Melbourne, Melbourne 3052, Australia
11 Neuroscience Center, Indiana University School of Medicine at Indianapolis, Indiana, IN 46202, USA
12 DZNE-German Center for Neurodegenerative Diseases, Tübingen 72076, Germany
13 Department of Neurology, Ludwig-Maximilians-University, Munich 80539, Germany
14 German Center for Neurodegenerative Diseases, Munich 81377, Germany
15 Munich Cluster for Systems Neurology (SyNergy), Munich 81377, Germany
16 Memory & Aging Program, Butler Hospital, Brown University in Providence, RI 02906, USA
17 Dementia Research Centre, Department of Neurodegenerative Disease, University College London Institute of Neurology, London WC1N 3BG, UK
18 Department of Neurology, Mayo Clinic Florida, Jacksonville, FL 33224, USA
19 Department of Radiology and Biomedical Imaging, University of California, San Francisco, CA 94143, USA

Correspondence to: Gil Rabinovici, MD
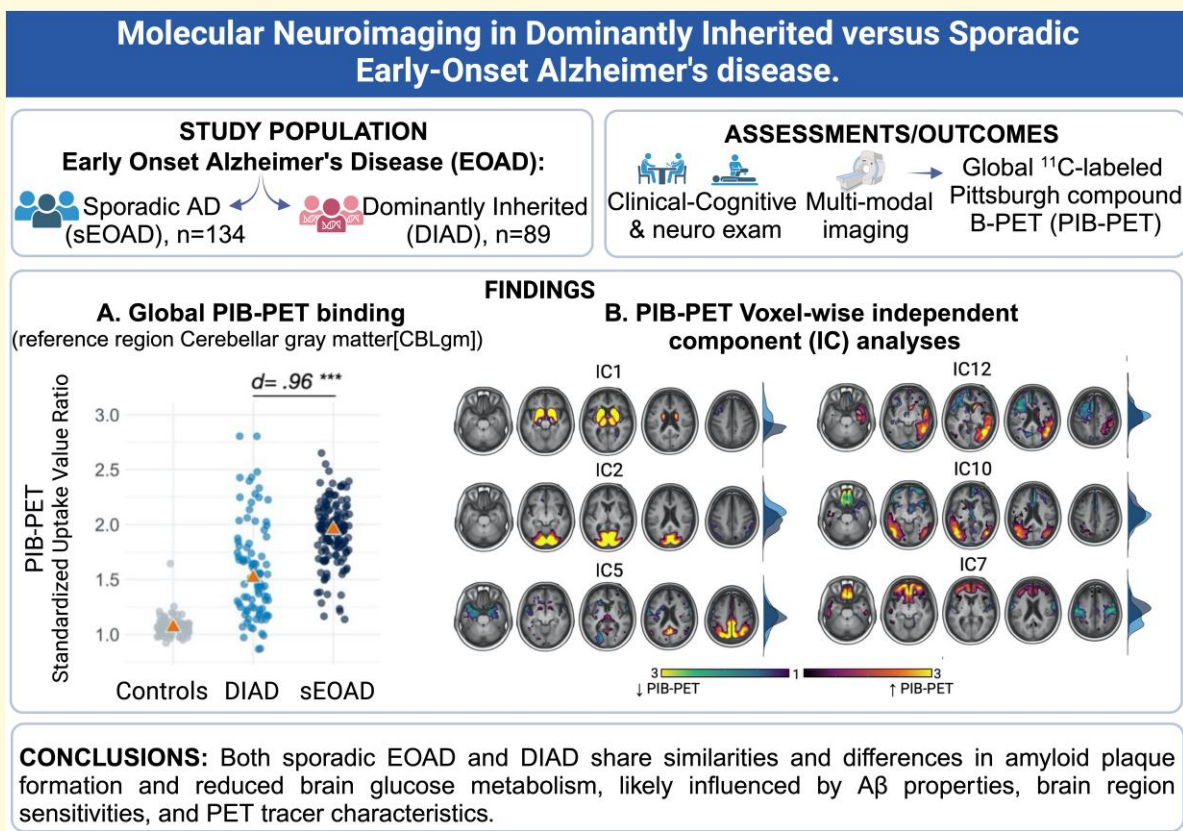Memory and Aging Center, Department of Neurology
Weill Institute for Neurosciences, University of California San Francisco
675 Nelson Rising Lane, Suite 190 San Francisco, San Francisco, CA 94158, USA
E-mail: gil.rabinovici@ucsf.edu

Graphical Abstract

Introduction

Alzheimer's disease is the most common cause of dementia worldwide[1] and is biologically defined by pathological accumulation of amyloid-β (Aβ) plaques and neurofibrillary tau tangles.[2] Alzheimer's disease can be either sporadic or due to dominantly inherited mutations in the genes *Presinilin-1* (*PSEN1*), *PSEN2* or *Amyloid Precursor Protein* (*APP*). The majority of individuals with Alzheimer's disease develop symptoms in older age in the absence of a pathogenic gene mutation [sporadic late-onset Alzheimer's disease (LOAD)[3,4]]. Approximately 5% of patients develop symptoms before age 65 [early-onset Alzheimer's disease (EOAD)][5]—of these, approximately 5–10% have a dominantly inherited form of Alzheimer's disease (DIAD, most commonly due to mutations in *PSEN1*), and the rest have apparently sporadic EOAD (sEOAD)[6,7].[7-9]

Clinical studies comparing DIAD versus sporadic LOAD have found similar cognitive syndromes, although with more rapid cognitive decline[3] and a higher prevalence of motor manifestations (e.g. myoclonus and spasticity)[10-12] in DIAD. Biomarker studies have demonstrated that DIAD and sporadic LOAD may be associated with different Aβ species (lower CSF Aβ37, Aβ38 and Aβ39 in DIAD),[13] with DIAD patients also showing higher cortical tau-PET binding,[14,15] more severe

neurodegeneration in Alzheimer's disease signature and other regions[16-19] and more advanced neuropathology at autopsy.[20-25] As for amyloid-Positron Emission Tomography (PET) measures, these have been suggested to be largely comparable between DIAD and LOAD patients, especially in neocortical regions, with some evidence for relatively higher binding in basal ganglia in DIAD.[26] Comparisons of sporadic forms of Alzheimer's disease by age of onset similarly revealed accelerated cognitive decline,[27,28] differential Aβ species accumulation (lower CSF Aβ43),[29] higher cortical tau-PET binding,[30-35] more severe neurodegeneration[34,36-42] and more advanced pathology at autopsy in sEOAD compared with sporadic LOAD.[43-46] As for amyloid-PET measures, previous studies have overall demonstrated null or weak associations between magnitude and/or spatial extent of binding elevation and age in sporadic Alzheimer's disease.[34,35] The observation that DIAD and sEOAD share a younger age and similar clinical and biomarker profiles compared with sporadic LOAD is of particular importance, suggesting complex relationships among Alzheimer's disease pathology, age and genetic status.

These studies overall seem to suggest that clinical and biomarker trajectories, within the Alzheimer's disease pathophysiological cascade, may be modulated by age, both in sporadic and in DIAD patients. Still, there is limited evidence comparing imaging biomarkers among sEOAD and DIAD

Table 1 Demographic, clinical and biomarker summary

Group	CN	sEOAD	DIAD	Effect size	P_{FDR}
Cohort	DIAN	UCSF	DIAN	-	-
Sample size—*N*	102	134	89	-	-
Age at PET (years)	44.9 (9.2)	59.7 (5.6)	45.8 (9.3)	1.91	<0.001
Age at onset (years)	-	54.8 (5.3)	41.9 (8.2)	1.96	<0.001
Sex—*N* (%) female	60 (58.8%)	76 (56.7%)	53 (59.5%)	0.03	0.8
Symptom duration (years)	-	4.9 (2.8)	4.1 (3.5)	0.26	0.09
Education (years)	14.6 (2.6)	16.4 (2.8)	13.5 (3.2)	1	<0.001
CDR-SB	0.03 (0.18)	4.48 (2.26)	5.73 (5.5)	0.32	0.06
MMSE	29.2 (1.1)	20.6 (6.1)	21.2 (7.4)	0.08	0.6
Global cortical PIB-PET SUVR	1.07 (0.08)	1.92 (0.29)	1.58 (0.44)	0.96	<0.001
PIB-PET Centiloid values	−3 (9)	94 (32)	55 (50)	0.96	<0.001
Global cortical FDG-PET SUVR	1.56 (0.13)	1.32 (0.1)	1.39 (0.19)	0.48	**0.002**
CDR total score | N 0/0.5/1/2/3	102/0/0/0/0	0/61/68/2/1	0/51/20/15/3	0.37	<0.001
APOE ε4 Status—*N* (%) carrier	35 (34.3%)	71 (54.6%)	25 (28.1%)	0.26	<0.001
DIAD gene | *PSEN1/PSEN2/APP*	-	-	75/2/12	-	-
FDG-PET Available—*N*(%)	87 (85.3%)	113 (84.3%)	88 (98.9%)	0.24	**0.001**

Table shows demographic, clinical and biomarker summary split by cohorts. Effect sizes and *P*-values refer to sEOAD versus DIAD comparisons, values displayed in bold indicate statistically significant differences. Continuous variables are presented as mean (SD). *P*-values are corrected with a FDR correction for multiple comparisons. Effect sizes were computed as Cohen's *d* for continuous variables and Cramer's *V* for discrete variables comparisons. Missing data: CDR total/sb was missing for *N* = 2 sEOAD participants. APOE ε4 Status was missing for *N* = 4 sEOAD participants. Education years info was missing for *N* = 26 CN, *N* = 13 DIAD and *N* = 1 sEOAD participants. MMSE was missing for *N* = 1 CN and *N* = 2 sEOAD participants. FDG-PET data were missing for *N* = 15 CN, *N* = 1 DIAD and *N* = 21 sEOAD participants. CN, cognitively normal; sEOAD, sporadic early-onset Alzheimer's disease; DIAD, dominantly inherited Alzheimer's disease; FDR, false discovery rate; DIAN, Dominantly Inherited Alzheimer Network; UCSF, University of California San Francisco; CDR sb, Clinical Dementia Rating sum of boxes; MMSE, Mini-Mental State Examination; APOE, apolipoprotein E; PSEN1, Presinilin-1; PSEN2, Presinilin-2; APP, Amyloid Precursor Protein.

groups, potentially more directly uncovering Alzheimer's disease pathophysiological differences less related to age and more likely to be associated to genetic status. In this study, we directly compared a sEOAD cohort followed at the University of California San Francisco Alzheimer's Disease Research Center (UCSF ADRC) and a cohort of DIAD individuals from the multi-site Dominantly Inherited Alzheimer Network (DIAN). Within this collaborative study, we systematically compared available PET imaging biomarkers [i.e. ^{11}C-Pittsburgh Compound B (PIB)-PET (PIB-PET, targeting Aβ accumulation) and ^{18}F-fluorodeoxyglucose (^{18}F-FDG)-PET (FDG-PET, targeting brain glucose metabolism)]. A complementary comparison of clinical and cognitive measures and fluid biomarkers is reported in a separate manuscript.[47] We aimed to (i) compare global imaging metrics and voxel-level PIB-PET and FDG-PET binding in sEOAD versus DIAD and (ii) identify independent PIB-PET and FDG-PET binding patterns in symptomatic participants and compare their expression in the two groups.

Materials and methods

Participants

Inclusion criteria

sEOAD cohort

sEOAD participants from the UCSF ADRC were required to (i) have an available and positive PIB-PET scan to establish Alzheimer's continuum,[48] (ii) have undergone a detailed neurological and neuropsychological examination, (iii) be symptomatic [Clinical Dementia Rating (CDR®) total score ≥ 0.5] at PIB-PET time, (iv) have age at reported symptoms onset

< 65 years old, (v) have absence of a family history of dementia that followed an autosomal dominant pattern and did not have evidence of a mutation associated with DIAD and (vi) have a clinical diagnosis of MCI or dementia due to Alzheimer's disease.[49,50] PIB-PET positivity in the sEOAD group was assessed both at visual read and quantitation as previously described.[51]

DIAD cohort

DIAD participants were required to (i) have an available PIB-PET scan, (ii) have undergone a detailed neurological and neuropsychological examination, (iii) be symptomatic (CDR® total score ≥ 0.5) at PIB-PET time, (iv) have age at reported symptoms onset < 65 years old and (v) carry a known dominantly inherited pathogenic mutation in *PSEN1*, *PSEN2* or *APP* to establish Alzheimer's disease. Detailed inclusion criteria for the parent DIAN study are available at https://dian.wustl.edu.

CN cohort

Cognitively unimpaired (global CDR = 0) non-mutation carriers DIAN participants with an available PIB-PET scan were included in the present study as a cognitively normal (CN) control. CN controls underwent the same diagnostic procedures as DIAD participants.

All participants had available demographics, neurological and neuropsychological examinations. For DIAD participants, PIB-PET, FDG-PET and structural MRI were acquired at the same visit of the clinical and cognitive assessment (DIAD). For sEOAD participants, PIB-PET, FDG-PET and structural MRI were acquired within 1 year from the clinical and cognitive assessment. FDG-PET was available for ~88% of the participants, and apolipoprotein E (*APOE*) genotyping data were also available for ~99% of participants (see below and Table 1).

Data selection

sEOAD cohort

Data querying (March 2019) identified $N = 134$ sEOAD participants meeting inclusion criteria, all recruited from the UCSF ADRC between 2005 and 2019. Two participants did not have CDR available but had Mini-Mental State Examination (MMSE) scores < 24 and were thus included as symptomatic. FDG-PET scans were available for 113/134 ($\sim$84%) sEOAD. All the PIB-PET scans included for the sEOAD cohort were baseline scans.

DIAD and CN cohorts

Data from DIAN Data Freeze 13 were included. For this analysis, we included DIAD symptomatic participants and asymptomatic non-mutation carriers as controls. Querying for participants with a complete PIB-PET scan passing quality control, we found $N = 326$ visits belonging to $N = 211$ ($N = 110/211$ non-mutation carriers and $N = 101/211$ mutation carriers) unique participants. As DIAN participants were on average younger than sEOAD participants, we selected the latest PIB-PET time point available for the $N = 211$ participants, i.e. selecting the last visit in case multiple visits were available. Considering the last visits, non-mutation carriers with a CDR total score of >0 ($N = 8$) and mutation carriers with a CDR total score of 0 ($N = 12$) were excluded. This resulted in a total of $N = 89$ symptomatic mutation carriers (DIAD group) and $N = 102$ CN non-mutation carriers (CN group). FDG-PET scans were available for 88/89 ($\sim$99%) DIAD and 87/102 ($\sim$85%) CN participants. There were no mutation carriers with the APP E693Q variant (Dutch type CAA), which has previously been shown to demonstrate minimal PIB-PET abnormalities and a different clinical progression.

MRI acquisition

sEOAD cohort

Structural MRIs were acquired either at the UCSF Neuroimaging Center ($N = 109/134$) or at the San Francisco Veterans Affairs Medical Centre ($N = 25/134$) as high-resolution T_1-weighted magnetization-prepared rapid gradient echo sequences. UCSF Neuroimaging Center scans were performed on either a 3T Siemens Tim Trio scanner ($N = 61$) or on a 3T Siemens Prisma Fit ($N = 48$). San Francisco Veterans Affairs Medical Centre scans were performed on either a 1.5T Siemens VISION system ($N = 17$) or on a 4T Bruker MedSpec system controlled by a Siemens Trio console ($N = 8$). Specific acquisition parameters have been outlined previously.[34,52,53]

DIAD and CN cohorts

Details on study procedures are available on the DIAN website (https://dian.wustl.edu/). All MRI scans were performed on validated scanners by the participating sites and included a T_1-weighted magnetization-prepared rapid gradient echo scan that was used for further processing in the present study.

MRI processing

All structural MRIs used in the present study (regardless of cohort and/or scanner) underwent the same processing pipeline at UCSF, including rigid-body co-registration to a template MRI and processing with Freesurfer 7.1 (http://surfer.nmr.mgh.harvard.edu/), additionally using the brainstem substructures parcellation module.[54] MRIs were then segmented with SPM12 (https://www.fil.ion.ucl.ac.uk/spm/software/spm12/) saving forward deformation parameters. Quality control was performed on all MRI processing files to ensure correct parcellation and segmentation. While the FDG-PET acquisitions were more compatible between UCSF and DIAN (see below), the structural MRI acquisitions were largely heterogeneous across participants and cohorts and were thus not considered for further statistical analyses but only used to process PET scans (see below).

PET acquisition

sEOAD cohort

PIB-PET and FDG-PET were acquired at the Lawrence Berkeley National Laboratory (Berkeley, CA, USA) with either a Siemens ECAT EXACT HR ($N = 45$ FDG-PET; $N = 47$ PIB-PET) or a Siemens Biograph 6 Truepoint PET/CT scanner in 3D acquisition mode ($N = 68$ FDG-PET; $N = 87$ PIB-PET). Attenuation correction was performed using a low-dose CT/transmission scan acquired prior to all the PET scans. For PIB-PET, dynamic acquisition was performed for 90 min (35 frames total) immediately after intravenous injection of $\sim$15 mCi of ^{11}C-PiB. For FDG-PET, a 30-min scan (6×5 min frames) was acquired 30 min following i.v. injection of 5–10 mCi of ^{18}F-FDG (resting quietly with eyes open during acquisition). All images were acquired in list mode and reconstructed using an ordered subset expectation maximum algorithm with weighted attenuation. Biograph and ECAT images were smoothed using a 4-mm Gaussian kernel with scatter correction during reconstruction (calculated image resolution Biograph $6.5 \times 6.5 \times 7.25$ mm, ECAT $7 \times 7 \times 7.5$ mm using Hoffman phantom).

DIAD and CN cohorts

Details on study procedures are available on the DIAN website (https://dian.wustl.edu/). Available dynamic PIB-PET and FDG-PET scans were downloaded in their original format for further processing. For both tracers, only data with the expected acquisition protocol were included for further processing. For PIB-PET, this included a 33-frame, 70-min-long dynamic scan starting at time of injection or a 6-frame, 30-min-long dynamic scan starting 40 min post-injection of 8–18 mCi (min-max) of ^{11}C-PiB. For FDG-PET, the scan was performed as a 6-frame, 30-min-long acquisition starting 30 min post-injection of 5 ± 0.5 mCi of ^{18}F-FDG.

PET pre-processing

PET data from UCSF and DIAN cohorts underwent the same pre-processing pipeline at UCSF regardless of cohort and/or scanner. Frames representing 50–70 min post-injection for PIB-PET and 30–60 min post-injection for FDG-PET were selected, rigidly realigned and averaged. A differential smoothing approach was then applied to bring all the PET images to an estimated 8-mm^3 resolution, using scanner-specific values as provided in DIAN for the DIAD cohort and as calculated for the sEOAD cohort based on Hoffman phantom acquisitions. Reference regions were defined via Freesurfer and the brainstem parcellation module to identify cerebellar grey matter (for PIB-PET) and pons (for FDG-PET). Averaged, smoothed PET scans were co-registered to their respective structural MRIs and intensity normalized according to average reference region binding, generating standardized uptake value ratio (SUVR) images for both PIB-PET ($SUVR_{50-70}$) and FDG-PET ($SUVR_{30-60}$) images. PET SUVR images were warped to the Montreal Neurological Institute space using the deformation parameters generated by the SPM12 segmentation of the respective structural MRI. For voxelwise analysis, an explicit mask was generated by averaging whole group warped grey and white matter segmentations, thresholding the image at >0.2 and manually removing the brainstem and cerebellum.

PET analysis

Global binding group-level comparisons

First, a summary average PIB-PET (cerebellar grey reference) and FDG-PET (pons reference) SUVR was estimated including all cortical regions (Desikan–Killiany atlas, https://surfer.nmr.mgh.harvard.edu/fswiki/CorticalParcellation) as defined by Freesurfer. We then tested additional combinations of target regions in order to investigate their relative impact on sEOAD versus DIAD comparisons. We first estimated average binding in a more restricted neocortical target region including frontal, temporal and parietal regions, using cerebellar grey as a reference, which has been our default approach to investigate binding in Alzheimer's disease-related regions.[51] To avoid bias related to the exclusion of striatal/subcortical binding, possibly leading to systematic underestimations in DIAD, we then tried more inclusive target masks considering the cortical regions described above plus (i) basal ganglia and (ii) basal ganglia, occipital lobe and thalamus.

Voxelwise group-level comparisons

Voxelwise analyses were performed with SPM12 to compare PIB-PET and FDG-PET binding across groups. The statistical threshold was set *a priori* to be $P < 0.001$ uncorrected for multiple comparisons. Family-wise error correction to $P < 0.05$ at the cluster level was used as an additional thresholding approach. Thresholded spm-T images were converted to Cohen's *d* effect sizes images with the Computational Anatomy Toolbox (CAT12) for SPM12 (http://www.neuro.uni-jena.de/cat/). Symptomatic participants (both sEOAD and DIAD) were compared to CN correcting for age and sex. When comparing sEOAD versus DIAD participants, multiple combinations of additional covariates were included to test their relative impact on the model, including MMSE, APOE ϵ4 status and respective global cortical biomarker binding.

Voxelwise ICAs

To investigate whether sEOAD and DIAD differed with regard to differential expression of binding patterns, we performed a group independent component analysis (ICA), including scans from both groups, separately for PIB-PET and FDG-PET, with the GIFT toolbox (https://trendscenter.org/software/gift/). A number of components were estimated through the minimum description length (i.i.d sampling) implementation in the toolbox, resulting in $N = 6$ estimated components for FDG-PET and $N = 12$ components for PIB-PET. Analysis was run using the Infomax method to define components and ICASSO with $N = 10$ runs. Both bootstrapping and random initiation were used to select a stable run. All the other settings and parameters were set to defaults. To avoid spatially biased results, images with a restricted field of view were excluded from this analysis, and all images were masked to only keep grey/white matter tissue prior to running the analysis. Resulting component maps were visually inspected and selected if they appeared not artefactual (e.g. ring effects).[55] Loading coefficients for each subject and component were then compared across sEOAD and DIAD groups with and without the same set of covariates mentioned above to test differences.

Statistical analysis

Group comparisons of continuous variables between sEOAD, DIAD and CN were tested by ANOVA followed by pairwise Tukey honestly significant difference *post hoc* comparisons. Differences in frequencies for qualitative variables were tested with a chi-squared (χ^2) test. Effect sizes for sEOAD versus DIAD comparisons were calculated with Cohen's *d* for continuous variables and Cramer's *V* for discrete variables. All *P*-values were corrected for multiple comparisons with a false discovery rate (FDR) correction. Adjusted group comparisons between loading parameters estimated in the ICA were run using a general linear model with all possible combinations of five covariates of nuisance, including age, sex, MMSE, APOE ϵ4 status and respective global cortical binding (replicating the voxelwise approach). Partial η^2 and respective *P*-values were generated for each of these analyses relative to the group factor. Plotting of voxelwise analysis was done via MRIcroGL software (https://www.nitrc.org/projects/mricrogl). Colour scales were chosen to be perceptually stable. The remaining plotting was performed in R (v4.0.2) with ggplot2.[56]

Sensitivity analyses

We ran two different sets of sensitivity analyses. First, considering some evidence for higher cerebellar PIB-PET binding in DIAD, all the global binding and voxelwise group-level

comparisons were repeated using pons as the reference region. Second, the original study inclusion criteria required only sEOAD to be amyloid positive, with no specific amyloid status requirement for DIAN participants. Given that this choice could have biased the PIB-PET comparisons, we repeated the global binding analyses after excluding $N = 2$ amyloid-positive CN and $N = 9$ amyloid-negative DIAD participants, as defined by the A ± status provided by the DIAN PET Core (approach described in Su et al.[57]). Additionally, DIAN participants lacking an available DIAN PETCore A ± status at the study time point were also excluded ($N = 7$, $N = 1$ CN and $N = 6$ symptomatic DIAD). This sensitivity analysis was thus performed on a sample including $N = 99$ amyloid-negative CN, $N = 74$ amyloid-positive symptomatic DIAD and $N = 134$ amyloid-positive sEOAD participants.

Results

sEOAD participants were on average 14 years older at PIB-PET ($d = 1.91$, $P_{FDR} < 0.001$) and 13 years older at symptom onset ($d = 1.96$, $P_{FDR} < 0.001$) than DIAD participants. sEOAD participants had on average 3 more years of education ($d = 1$, $P_{FDR} < 0.001$) than DIAD participants and were more likely to be APOE ε4 carriers (55% versus 28%, $V = 0.26$, $P_{FDR} < 0.001$). The distribution of global CDR total scores at PET was significantly different between groups, with the DIAD group having relatively more moderate/severe cases ($V = 0.37$, $P_{FDR} < 0.001$), and CDR sum of boxes was higher in DIAD ($d = 0.32$, $P_{FDR} = 0.06$). sEOAD and DIAD groups did not differ in sex ($V = 0.03$, $P_{FDR} = 0.8$), symptom duration ($d = 0.26$, $P_{FDR} = 0.09$), CDR sum of boxes scores and MMSE ($d = 0.33$, $P_{FDR} = 0.06$; $d = 0.08$, $P_{FDR} = 0.6$, respectively). See Table 1 for details.

Global binding group-level comparisons

sEOAD participants had on average higher whole cortical PIB-PET ($d = 0.96$, $P_{FDR} < 0.001$; see Fig. 1) and lower whole cortical FDG-PET ($d = 0.48$; $P_{FDR} = 0.002$) binding compared with DIAD. Converted Centiloid values from the whole cortical PIB-PET SUVR, with cerebellar reference, were mean ± SD $94 ± 32$ in sEOAD and $55 ± 50$ in DIAD (see the supplementary materials for Centiloid conversion validation). PIB-PET differences remained significant after adjusting for various combinations of age, sex, MMSE and APOE ε4 status covariates. FDG-PET differences remained significant when correcting for sex but not in the other models (see Supplementary Table 1). PIB-PET differences also remained significant with different target regions, ranging from the greatest magnitude using a default cortical target with cerebellar reference ($d = 0.98$, $P_{FDR} < 0.001$) to the smallest magnitude
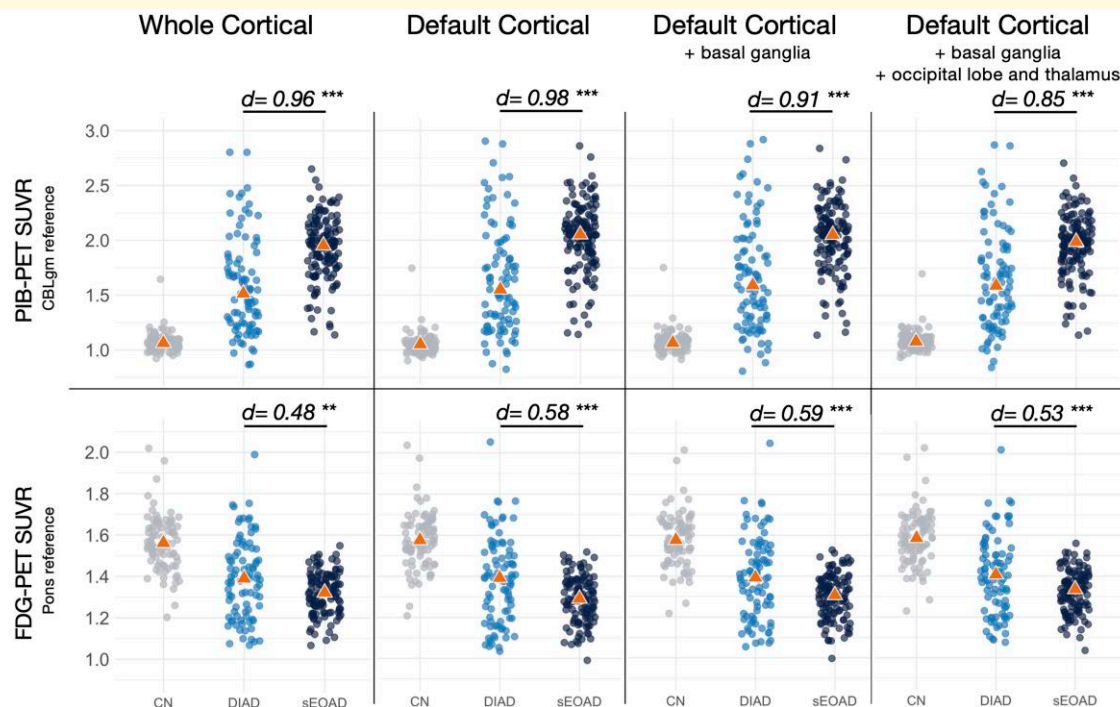

Figure 1 Global binding group-level comparisons by target region. Legend: Figure showing distribution of PIB-PET SUVR and FDG-PET SUVR values according to group, with four different target regions (see text for details). See text for more details. Each point represents a participant. CBLgm, cerebellar grey matter; d, Cohen's d; ***P < 0.001; **P < 0.01; CN, cognitively normal; DIAD, dominantly inherited Alzheimer's disease (symptomatic participants); sEOAD, sporadic early-onset Alzheimer's disease; FDG, ^{18}F-fluorodeoxyglucose; PIB, Pittsburgh Compound B; SUVR, standardized uptake value ratio.

Figure 2 Voxelwise group-level comparisons with different sets of covariates. Legend: Figure showing voxelwise group comparisons results between sEOAD/DIAD and CN groups (top two rows) and between sEOAD and DIAD participants (bottom five rows). For the DIAD versus sEOAD comparisons, models adjusted with different sets of covariates are shown. Colour scales represent Cohen's *d* effect sizes; see main text for details. Images are generated with mricroGL software. *d*, Cohen's *d*; CN, cognitively normal; DIAD, dominantly inherited Alzheimer's disease; sEOAD, sporadic early-onset Alzheimer's disease; MMSE, Mini-Mental State Examination; APOE, apolipoprotein E; FDG, ^{18}F-fluorodeoxyglucose; PIB, Pittsburgh Compound B.

using the most comprehensive target region including default regions plus basal ganglia, occipital lobe and thalamus ($d = 0.85$, $P_{FDR} < 0.001$); see Fig. 1 for details. Within DIAD participants, global binding estimations varied between and within mutated genes (see Supplementary Fig. 1). Several DIAD participants presented with a seemingly negative amyloid-PET scan (see Fig. 1 and 'Sensitivity analysis' section below). In a subset analysis, selecting only the PSEN-1 variants with mutations occurring prior to codon < 200, the differences for whole cortical PIB-PET biding were not significant compared with the sEOAD ($P = 0.17$) (see Supplementary Fig. 1).

Voxelwise group-level comparisons

Both sEOAD and DIAD groups showed elevated PIB-PET and reduced FDG-PET compared with the CN group, with sEOAD overall showing greater effect sizes but similar spatial patterns (Fig. 2). When comparing sEOAD versus DIAD directly, the fully adjusted models showed significant tracer-specific regional differences. For PIB-PET, DIAD showed relatively greater binding in occipital, frontal and subcortical regions, including caudate, putamen and thalamus, whereas sEOAD participants showed relatively greater binding
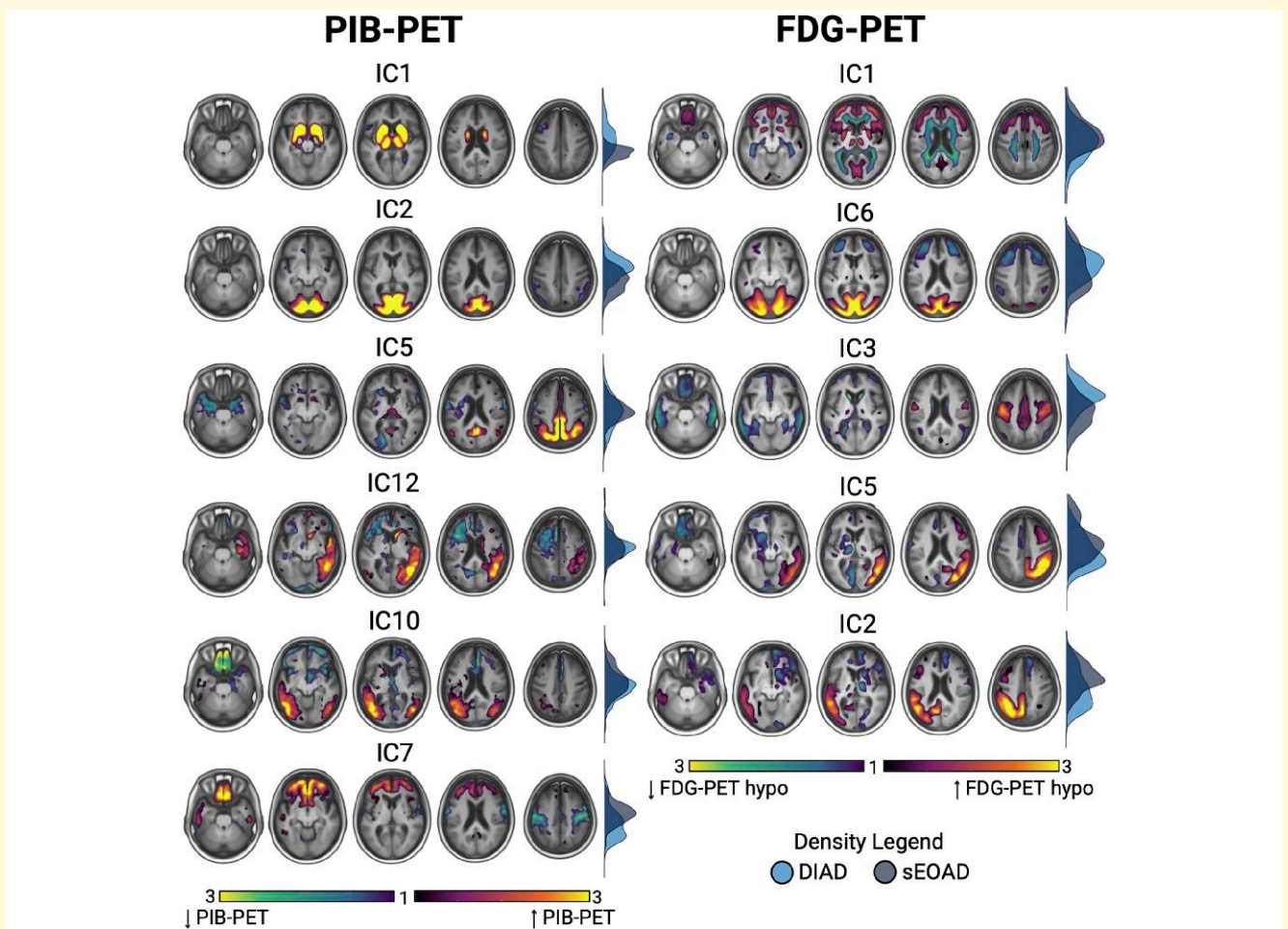
Figure 3 Voxelwise ICA. Legend: Figure showing results of the ICAs. Brain renderings show components for both PIB-PET (left) and FDG-PET (right), with colour scales representing z-scored contributions of each voxel to the respective component. Components were thresholded to |z| > 1 for visualization. Density plots for each component represent distribution of loading parameters between DIAD and sEOAD participants. Images are generated with mricroGL software. IC, independent component; DIAD, dominantly inherited Alzheimer's disease; sEOAD, sporadic early-onset Alzheimer's disease; FDG, ^{18}F-fluorodeoxyglucose; PIB, Pittsburgh Compound B.

restricted to WM. For FDG-PET, sEOAD participants showed greater hypometabolism in Alzheimer's disease signature regions and the caudate nuclei, with DIAD instead showing greater hypometabolism in precentral, medial frontal areas and occipital regions. These observed differences showed some variation with the inclusion of different combinations of covariates (see Fig. 2).

Voxelwise ICA

Six components for PIB-PET and five components for FDG-PET were selected after visual inspection (see Fig. 3). For PIB-PET, unadjusted comparisons of loading parameters showed that DIAD participants on average expressed more significantly the basal ganglia (IC1, $d = 1.54$, $P_{FDR} < 0.001$) and occipital (IC2, $d = 1.12$, $P_{FDR} < 0.001$) components, whereas sEOAD participants expressed more significantly the frontal (IC7, $d = 0.82$, $P_{FDR} < 0.001$) and left temporoparietal components (IC10, $d = 0.53$, $P_{FDR} < 0.001$). The bilateral

superior parietal (IC5) and the right temporoparietal (IC12) components were similarly expressed in the two groups ($d = 0.06$, $P_{FDR} = 0.7$; $d = 0.13$, $P_{FDR} = 0.4$, respectively). For FDG-PET, DIAD participants expressed more significantly the pericentral (IC3, $d = 1.12$, $P_{FDR} < 0.001$) component, whereas sEOAD participants expressed more significantly the frontal (IC1, $d = 0.60$, $P_{FDR} < 0.001$), left temporo-parieto-frontal (IC2, $d = 0.69$, $P_{FDR} < 0.001$) and right temporo-parieto-frontal (IC5, $d = 0.65$, $P_{FDR} < 0.001$) components. The occipital component was expressed similarly in both groups, with a trend towards higher expression in DIAD ($d = 0.28$, $P_{FDR} = 0.06$). See Fig. 4 for the distribution of loadings for both PIB-PET and FDG-PET components. Differences for the basal ganglia and occipital PIB-PET components and for the pericentral and right temporo-parieto-frontal FDG-PET components remained significant after adjusting for various combinations of age, sex, MMSE, *APOE* ε4 status and respective global cortical binding (see Supplementary Table 2). Supplementary Fig. 4 shows in more detail the distribution of
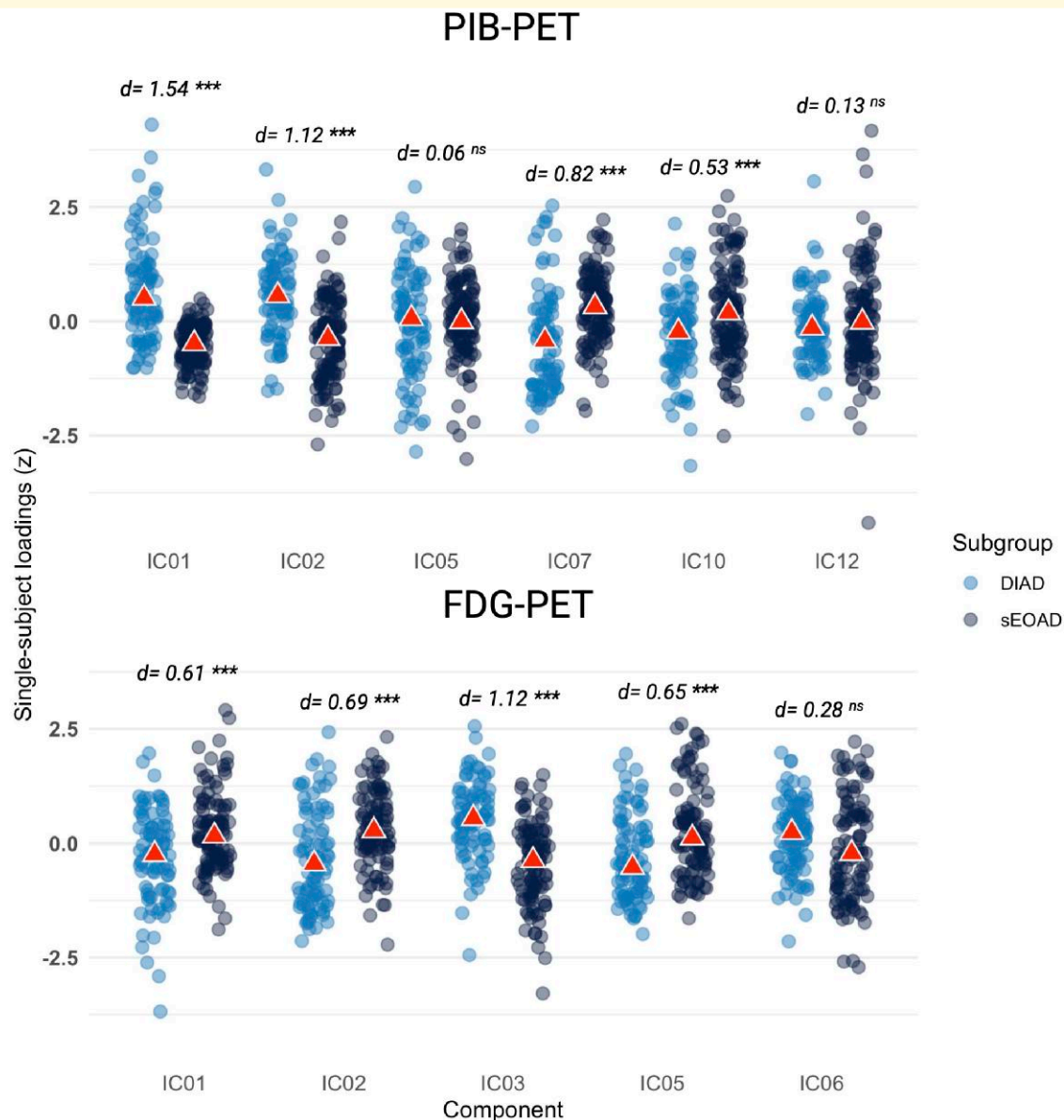
Figure 4 Distribution of loadings for PIB-PET and FDG-PET components. Legend: Figure showing distribution of loadings in sEOAD and DIAD participants for all the identified PIB-PET and FDG-PET components. Triangles indicate respective medians. Effect size and significance refer to crude (unadjusted) comparisons. Each point represents a participant. *d*, Cohen's *d*; ***P_{FDR} < 0.001; ns, non-significant; IC, independent component; DIAD, dominantly inherited Alzheimer's disease; sEOAD, sporadic early-onset Alzheimer's disease; FDG, ^{18}F-fluorodeoxyglucose; PIB, Pittsburgh Compound B.

scores across the four components significant in adjusted models, labelling DIAD patients showing the highest loadings according to their mutation.

Sensitivity analyses

PIB-PET differences were attenuated but still significant when repeated using the pons as reference, across the different target regions in the global analysis (Supplementary Fig. 2) as well as in the voxelwise models (Supplementary Fig. 3). sEOAD participants still showed higher global PIB-PET binding compared with symptomatic amyloid-positive DIAD patients

with a greater magnitude of difference using cerebellum versus pons reference regions. As in the main analysis, adding basal ganglia, occipital and thalamic regions to the global PIB region of interest attenuated group differences, as did the use of the pons as the reference region (Cohen's *d* range 0.86–0.24, P_{FDR} range < 0.001–0.15; see Supplementary Fig. 5).

Discussion

sEOAD and DIAD patients showed overlap and also significant differences in both PIB-PET and FDG-PET binding patterns.

PiB-PET retention, a measure of Aβ plaque accumulation, largely converged in the same regions for both groups, with particularly pronounced involvement of subcortical structures in dominantly inherited cases. Brain glucose hypometabolism in pericentral and medial frontal regions was relatively more pronounced in dominantly inherited rather than sporadic participants, whereas sEOAD showed relatively greater temporoparietal and caudate involvement. The present findings suggest that the presence or absence of known dominantly inherited mutations may influence Aβ plaque accumulation and brain glucose hypometabolism patterns in EOAD. Alternatively, Aβ plaque characteristics (e.g. cotton wool plaques) may differ according to DIAD variant, which may explain heterogeneity in PIB affinity and lower PIB-PET binding affinity in certain DIAD variants.

Previous studies have focused on differences between DIAD and LOAD, in which differences in age may be a significant confounder convolving age-related processes with possible differences due to mutation status. The present study was designed to compare DIAD and sEOAD cohorts sharing a younger age at symptom onset, thereby disentangling differences more likely to be related to dominantly inherited disease. Taking into account that DIAD participants were still significantly younger than the sEOAD participants, we found overall higher global PIB-PET binding in sEOAD compared with DIAD. The magnitude of this difference was influenced by the choice of target and reference regions but was overall consistent across methods and in line with previous reports.[26,58-63] The observed PIB-PET binding differences may also possibly reflect heterogeneity in relationships between symptom onset and amyloid duration/time, the latter potentially longer in sEOAD compared with DIAD.[64,65] In assessing differences in the spatial topography of amyloid deposition, voxelwise analyses (controlling for global PIB-PET binding, thus revealing regions relatively more involved) demonstrated that DIAD showed greater involvement of striatum and thalamus, as well as the occipital pericalcarine region and the frontal pole, with sEOAD patients showing higher white matter PIB-PET binding. The striatum is known to be involved early in DIAD,[58,62,66-71] even before detectable cortical accumulation,[58,62,66-68] with the thalamus also recognized as a key structure in the progression of DIAD.[19,59,71] This is in contrast with the relatively late detection of significant amyloid-PET binding in the striatum in patients with sporadic Alzheimer's disease.[67,72,73] Similar findings were previously reported in vivo with PIB-PET in a smaller cohort including a mix of sporadic LOAD and EOAD and DIAD PSEN1 mutation carriers,[59] with structural MRI providing converging evidence for greater thalamic volume loss in DIAD versus sEOAD in an independent study.[74] Concordant evidence was also reported in a previous autopsy study, which examined sporadic LOAD and a mix of APP and PSEN1 DIAD patients, finding more severe striatal Aβ42 accumulation in DIAD and more severe cortical Aβ42 accumulation in sporadic Alzheimer's disease.[75] Although mutation carriers with the APP E693Q variant (Dutch-type CAA) were not included in this analysis, greater PIB binding in occipital regions in DIAD could be related to underlying cerebral amyloid angiopathy,[76,77] which shows a predilection for occipital cortex and can be more severe in DIAD compared with sEOAD.[78] In particular, PSEN1 mutations occurring after codon 200 more frequently associate with amyloid angiopathy and parenchymal amyloid accumulation including both diffuse and cored plaques.[79] It is difficult to interpret the relatively higher white matter PIB-PET binding observed in sEOAD compared with DIAD. It has been proposed that amyloid-PET ligand binding in white matter may be associated with myelin or myelin-associated proteins, with lower binding seen in regions that show T2/FLAIR white matter hyperintensities on MRI.[80-82] Our observation could thus indicate greater white matter pathology in the DIAD group,[83,84] although further work is needed to understand the biological substrate of the detected differences in white matter binding. Overall, our findings suggest that, within the Alzheimer's disease spectrum, genetic determinants influence the topography and magnitude of PIB-PET binding patterns.

Differences in the degree and spatial patterns of PIB-PET binding between DIAD and sEOAD may in part be related to mutation-specific differences in Aβ fibril microstructure and available binding sites[26,85,86] rather than differences in the burden or distribution of Aβ pathology per se. Specific DIAD mutations lead to 'cotton wool' amyloid plaques, which show an absent-to-low affinity for PIB binding.[85] Additionally, PIB-PET binding in Alzheimer's disease signature regions may be reflecting different amyloid pathology in DIAD versus sporadic Alzheimer's disease, namely diffuse plaques in the former and a combination of diffuse and cored plaques in the latter.[26] It is also possible that different brain regions may have greater susceptibility to the mechanisms posited to trigger Aβ plaque accumulation, i.e. overproduction of Aβ peptides in DIAD versus reduced clearance of Aβ in sporadic Alzheimer's disease.[87-90] In keeping with this hypothesis, a previous study has found that regional Aβ42 levels at autopsy correlated with synaptic markers in sporadic Alzheimer's disease but with the APP/β-C-terminal fragment of APP in DIAD.[75]

Within the DIAD group, we found further evidence of how different mutations lead to different patterns of Aβ plaque accumulation.[91] We observed heterogeneity in PIB-PET binding patterns, implying that not only mutation status but also mutation position (e.g. within the PSEN1 gene) may influence regional vulnerability to Aβ pathology. This confirms previous observations[59,62,91] and could indicate that different mutations may generate downstream Aβ pathology with distinct conformations, biochemical properties and regional distributions. Amyloid pathology heterogeneity in DIAD has also been reported in autopsy studies,[78,79,92,93] demonstrating that PSEN1 individuals with mutations occurring after codon 200 show more cored plaques and more amyloid angiopathy and that individuals with missense APP mutations show greater plaque formation than individuals with APP duplication, with APP individuals in general showing more severe Aβ40 angiopathy. Finally, a previous in vitro study has demonstrated that the Aβ42 and Aβ40 production potential differed across various mutant PSEN1 proteins.[94,95] Previous studies have also highlighted how, even within the same families, the

same mutation may present with different PET binding patterns, pathology and clinical profiles.[96-98] Finally, in our population, a few symptomatic DIAD mutation carriers presented with a seemingly negative amyloid-PET scan. This has been described previously[63,99-101] and may be associated with an Aβ pathology type being under-detected by PIB-PET (e.g. cotton wool plaques), amyloid accumulation in the cerebellar/pontine reference regions leading to low SUVR values[26] or symptoms in DIAD individuals that are not directly related to Aβ pathology.[26,85] Overall, our data demonstrate that the ability to quantify amyloid burden with PIB-PET likely varies according to the specific DIAD mutation and may explain observed differences within DIAD variants (codon <200 versus >200) and in relation to sEOAD. Previous studies in the DIAN cohort suggest that PIB-PET has limited ability to detect Aβ aggregates in cotton wool plaques and may underestimate the total Aβ plaque burden in brain regions with abundant cotton wool plaques. *PSEN1* mutations occurring after codon 200 have been reported to have a higher frequency of cotton wool plaques relative to those occurring before codon 200, and our study shows that *PSEN1* > 200 codon mutations also tend to present overall lower PIB-PET SUVR.

Adjusting for global cortical glucose metabolism, DIAD participants showed greater hypometabolism in the medial occipital, thalamic and pericentral cortex. sEOAD participants showed greater hypometabolism in Alzheimer's disease signature temporoparietal regions as well as the caudate nucleus, consistent with previously described greater involvement of subcortical structures in sEOAD compared with sporadic LOAD.[102] The discordance between significant Aβ pathology and lack of concomitant neurodegeneration in some subcortical structures (e.g. the caudate nuclei) in DIAD is consistent with previous observations.[58,66,103] Greater pericentral hypometabolism in DIAD could be associated with motor cortex and spinal cord involvement in some DIAD mutations, manifesting clinically as spasticity, myelopathy or myoclonus.[10-12] Conversely, these structures are largely spared in sporadic Alzheimer's disease.[104-107] Interestingly, the DIAD participant expressing the highest loading for the pericentral FDG-PET component carried a mutation in *PSEN1* (Ser169Leu) that has been associated with clumsiness and myoclonus.[108] Our analyses also indicated that sEOAD patients more frequently expressed a right-dominant pattern of temporoparietal hypometabolism compared with DIAD patients. This is likely to be associated with a higher prevalence of atypical (i.e. non-amnestic) and asymmetric Alzheimer's disease clinical presentations in sEOAD compared with DIAD,[3,47] which are tightly associated with specific FDG-PET hypometabolism patterns.[34,109-111]

This study has several limitations. First, it remains to be fully elucidated whether observed differences in amyloid-PET patterns may reflect absolute differences in either presence, location or type of Aβ pathology. Autopsy studies have generally indicated more severe pathology in DIAD versus all age sporadic Alzheimer's disease.[21,92,96,112,113] Additionally, previous fluid biomarker studies have provided evidence for lower[114] or similar[13,47] CSF Aβ42 in DIAD versus sporadic Alzheimer's disease, although CSF Aβ37, Aβ38 and Aβ39

concentrations were reported to be lower in DIAD.[13] It is possible that the inconsistency between imaging-, fluid- and autopsy-based findings is associated with both operational factors (e.g. analytical pipelines, reference and target regions), as well as biological factors (e.g. differential sensitivity of amyloid-PET tracers to different Aβ aggregates, type of mutation and disease stage).[26,85,86] We tried to address these factors by considering different target and reference regions, as well as by running pattern-based analyses such as ICA, which overall provided convergent evidence. Second, this study likely suffers from sampling bias. sEOAD is frequently diagnosed years after symptom onset, with a sometimes unreliable estimation of the actual duration from symptom onset. Conversely, DIAD participants, especially in studies like DIAN, are prospectively followed before and after symptom onset and closely monitored, implying a very accurate estimation of symptom duration. Therefore, despite the similar duration of estimated symptoms from onset in sEOAD and DIAD groups in the present study, it is still possible that due to a recall bias, the sEOAD participants had a longer duration of symptomatic disease at the time of imaging, potentially contributing to some of the observed PIB-PET and FDG-PET differences. Notwithstanding this uncertainty, our analyses (i) incorporated chronological age at PIB-PET, thus using a reliably anchored covariate, and (ii) focused on relative pattern differences, which were by design unrelated to global PET binding. Third, CN participants included in the present study were asymptomatic, non-mutation carriers from DIAN and were significantly younger than our sEOAD patients. All our primary analyses, however, only involved direct comparisons between symptomatic participants. Fourth, the symptomatic DIAD group presented with intrinsic heterogeneity with regard to PIB-PET binding patterns, potentially associated with the given mutation. It is reasonable to expect that some DIAD mutations may present with overall higher PIB-PET binding compared to sEOAD, but larger sample sizes will be needed in order to systematically investigate this.

Conclusion

In conclusion, our findings indicate that sporadic and dominantly inherited EOAD show overlap and also important distinctions in patterns of Aβ plaque deposition and glucose hypometabolism. Amyloid-PET differences likely reflect the interplay between heterogeneity in the biochemical and microstructural properties of Aβ deposits, regional vulnerabilities and PET tracer binding properties. Future studies including additional biomarkers (e.g. tau- and neuroinflammation-PET) may provide further insights into common and distinct aspects of the Alzheimer's disease pathophysiological cascade in sporadic versus dominantly inherited disease.

Supplementary material

Supplementary material is available at *Brain Communications* online.

Acknowledgements

Funding

Competing interests

Roche, Johnson & Johnson and Merck. He serves as an associate editor for JAMA Neurology.

Data availability

Data supporting the findings of this study are available on request and will follow the policies of the DIAN (https://dian.wustl.edu) and of the UCSF ADRC (https://memory.ucsf.edu/research-trials/professional/open-science#Data-Sharing), both of which comply with the guidelines established by the Collaboration for Alzheimer's Prevention. Data are not publicly available in order to preserve the privacy of research participants.

References

1. Masters CL, Bateman R, Blennow K, Rowe CC, Sperling RA, Cummings JL. Alzheimer's disease. *Nat Rev Dis Primers*. 2015; 1(1):15056.
2. Querfurth HW, LaFerla FM. Alzheimer's Disease. *N Engl J Med*. 2010;362(4):329-344.
3. Bateman RJ, Aisen PS, De Strooper B, *et al*. Autosomal-dominant Alzheimer's disease: A review and proposal for the prevention of Alzheimer's disease. *Alzheimers Res Ther*. 2011;3(1):1.
4. Reitz C, Rogaeva E, Beecham GW. Late-onset vs nonmendelian early-onset Alzheimer disease: A distinction without a difference? *Neurol Genet*. 2020;6(5):e512.
5. Szigeti K, Doody RS. Should EOAD patients be included in clinical trials? *Alzheimers Res Ther*. 2011;3(1):4.
6. Campion D, Dumanchin C, Hannequin D, *et al*. Early-onset autosomal dominant Alzheimer disease: Prevalence, genetic heterogeneity, and mutation spectrum. *Am J Hum Genet*. 1999;65(3): 664-670.
7. Cacace R, Sleegers K, Van Broeckhoven C. Molecular genetics of early-onset Alzheimer's disease revisited. *Alzheimers Dement*. 2016;12(6):733-748.
8. Lanoiselée HM, Nicolas G, Wallon D, *et al*. APP, PSEN1, and PSEN2 mutations in early-onset Alzheimer disease: A genetic screening study of familial and sporadic cases. *PLoS Med*. 2017; 14(3):e1002270.
9. Neuner SM, Tcw J, Goate AM. Genetic architecture of Alzheimer's disease. *Neurobiol Dis*. 2020;143:104976.
10. Pilotto A, Padovani A, Borroni B. Clinical, biological, and imaging features of monogenic Alzheimer's disease. *BioMed Res Int*. 2013; 2013:689591.
11. Ryan NS, Nicholas JM, Weston PSJ, *et al*. Clinical phenotype and genetic associations in autosomal dominant familial Alzheimer's disease: A case series. *Lancet Neurol*. 2016;15(13):1326-1335.
12. Tang M, Ryman DC, McDade E, *et al*. Neurological manifestations of autosomal dominant familial Alzheimer's disease: A comparison of the published literature with the dominantly inherited Alzheimer network observational study (DIAN-OBS). *Lancet Neurol*. 2016;15(13):1317-1325.
13. Portelius E, Andreasson U, Ringman JM, *et al*. Distinct cerebrospinal fluid amyloid beta peptide signatures in sporadic and PSEN1 A431E-associated familial Alzheimer's disease. *Mol Neurodegener*. 2010;5:2.
14. Chen CD, Holden TR, Gordon BA, *et al*. Ante- and postmortem tau in autosomal dominant and late-onset Alzheimer's disease. *Ann Clin Transl Neurol*. 2020;7(12):2475-2480.
15. Gordon BA, Blazey TM, Christensen J, *et al*. Tau PET in autosomal dominant Alzheimer's disease: Relationship with cognition, dementia and other biomarkers. *Brain*. 2019;142(4):1063-1076.
16. Gregory GC, Macdonald V, Schofield PR, Kril JJ, Halliday GM. Differences in regional brain atrophy in genetic forms of Alzheimer's disease. *Neurobiol Aging*. 2006;27(3):387-393.
17. Dincer A, Gordon BA, Hari-Raj A, *et al*. Comparing cortical signatures of atrophy between late-onset and autosomal dominant Alzheimer disease. *NeuroImage Clin*. 2020;28:102491.
18. Cash DM, Ridgway GR, Liang Y, *et al*. The pattern of atrophy in familial Alzheimer disease: Volumetric MRI results from the DIAN study. *Neurology*. 2013;81(16):1425-1433.
19. Pardilla-Delgado E, Torrico-Teave H, Sanchez JS, *et al*. Associations between subregional thalamic volume and brain pathology in autosomal dominant Alzheimer's disease. *Brain Commun*. 2021;3(2):fcab101.
20. Nochlin D, van Belle G, Bird TD, Sumi SM. Comparison of the severity of neuropathologic changes in familial and sporadic Alzheimer's disease. *Alzheimer Dis Assoc Disord*. 1993;7(4):212-222.
21. Ringman JM, Monsell S, Ng DW, *et al*. Neuropathology of autosomal dominant Alzheimer disease in the national Alzheimer coordinating center database. *J Neuropathol Exp Neurol*. 2016; 75(3):284-290.
22. Cairns NJ, Perrin RJ, Franklin EE, *et al*. Neuropathologic assessment of participants in two multi-center longitudinal observational studies: The Alzheimer Disease Neuroimaging Initiative (ADNI) and the Dominantly Inherited Alzheimer Network (DIAN). *Neuropathology*. 2015;35(4):390-400.
23. Schöll M, Almkvist O, Bogdanovic N, *et al*. Time course of glucose metabolism in relation to cognitive performance and postmortem neuropathology in Met146Val PSEN1 mutation carriers. *J Alzheimers Dis*. 2011;24(3):495-506.
24. Lemere CA, Lopera F, Kosik KS, *et al*. The E280A presenilin 1 Alzheimer mutation produces increased A beta 42 deposition and severe cerebellar pathology. *Nat Med*. 1996;2(10):1146-1150.
25. Shepherd CE, Grace EM, Mann DMA, Halliday GM. Relationship between neuronal loss and "inflammatory plaques" in early onset Alzheimer's disease. *Neuropathol Appl Neurobiol*. 2007;33(3): 328-333.
26. Chen CD, Joseph-Mathurin N, Sinha N, *et al*. Comparing amyloid-β plaque burden with antemortem PiB PET in autosomal dominant and late-onset Alzheimer disease. *Acta Neuropathol*. 2021;142(4):689-706.
27. Koedam ELGE, Pijnenburg YAL, Deeg DJH, *et al*. Early-onset dementia is associated with higher mortality. *Dement Geriatr Cogn Disord*. 2008;26(2):147-152.
28. Wattmo C, Wallin ÅK. Early- versus late-onset Alzheimer's disease in clinical practice: Cognitive and global outcomes over 3 years. *Alzheimers Res Ther*. 2017;9(1):70.
29. Lauridsen C, Sando SB, Møller I, *et al*. Cerebrospinal fluid Aβ43 is reduced in early-onset compared to late-onset Alzheimer's disease, but has similar diagnostic accuracy to Aβ42. *Front Aging Neurosci*. 2017;9:210.
30. Ossenkoppele R, Schonhaut DR, Schöll M, *et al*. Tau PET patterns mirror clinical and neuroanatomical variability in Alzheimer's disease. *Brain*. 2016;139(5):1551-1567.
31. Cho H, Choi JY, Lee SH, *et al*. Excessive tau accumulation in the parieto-occipital cortex characterizes early-onset Alzheimer's disease. *Neurobiol Aging*. 2017;53:103-111.
32. Schöll M, Ossenkoppele R, Strandberg O, *et al*. Distinct ^{18}F-AV-1451 tau PET retention patterns in early- and late-onset Alzheimer's disease. *Brain*. 2017;140(9):2286-2294.
33. Whitwell JL, Martin P, Graff-Radford J, *et al*. The role of age on tau PET uptake and gray matter atrophy in atypical Alzheimer's disease. *Alzheimers Dement*. 2019;15(5):675-685.
34. Iaccarino L, La Joie R, Edwards L, *et al*. Spatial relationships between molecular pathology and neurodegeneration in the Alzheimer's disease continuum. *Cereb Cortex*. 2021;31(1):1-14.
35. La Joie R, Visani AV, Lesman-Segev OH, *et al*. Association of APOE4 and clinical variability in Alzheimer disease with the pattern of tau- and amyloid-PET. *Neurology*. 2021;96(5):e650-e661.

36. Salmon E, Collette F, Degueldre C, Lemaire C, Franck G. Voxel-based analysis of confounding effects of age and dementia severity on cerebral metabolism in Alzheimer's disease. *Hum Brain Mapp*. 2000;10(1):39-48.

37. Kim EJ, Cho SS, Jeong Y, *et al*. Glucose metabolism in early onset versus late onset Alzheimer's disease: An SPM analysis of 120 patients. *Brain*. 2005;128(Pt 8):1790-1801.

38. Rabinovici GD, Furst AJ, Alkalay A, *et al*. Increased metabolic vulnerability in early-onset Alzheimer's disease is not related to amyloid burden. *Brain*. 2010;133(Pt 2):512-528.

39. Kaiser NC, Melrose RJ, Liu C, *et al*. Neuropsychological and neuroimaging markers in early versus late-onset Alzheimer's disease. *Am J Alzheimers Dis Other Demen*. 2012;27(7):520-529.

40. Möller C, Vrenken H, Jiskoot L, *et al*. Different patterns of gray matter atrophy in early- and late-onset Alzheimer's disease. *Neurobiol Aging*. 2013;34(8):2014-2022.

41. Chiaravalloti A, Koch G, Toniolo S, *et al*. Comparison between early-onset and late-onset Alzheimer's disease patients with amnestic presentation: CSF and (18)F-FDG PET study. *Dement Geriatr Cogn Dis Extra*. 2016;6(1):108-119.

42. Aziz AL, Giusiano B, Joubert S, *et al*. Difference in imaging biomarkers of neurodegeneration between early and late-onset amnestic Alzheimer's disease. *Neurobiol Aging*. 2017;54:22-30.

43. Bigio EH, Hynan LS, Sontag E, Satumtira S, White CL. Synapse loss is greater in presenile than senile onset Alzheimer disease: Implications for the cognitive reserve hypothesis. *Neuropathol Appl Neurobiol*. 2002;28(3):218-227.

44. Marshall GA, Fairbanks LA, Tekin S, Vinters HV, Cummings JL. Early-onset Alzheimer's disease is associated with greater pathologic burden. *J Geriatr Psychiatry Neurol*. 2007;20(1):29-33.

45. Spina S, La Joie R, Petersen C, *et al*. Comorbid neuropathological diagnoses in early versus late-onset Alzheimer's disease. *Brain*. 2021;144(7):2186-2198.

46. Arai T, Ikeda K. Morphometrical comparison of neurofibrillary tangles and senile plaques in Alzheimer's disease and the senile dementia of Alzheimer type. *Neuropathology*. 1995;15(1–2):21-26.

47. Llibre-Guerra JJ, Iaccarino L, Coble D, *et al*. Longitudinal clinical, cognitive and biomarker profiles in dominantly inherited versus sporadic early-onset Alzheimer's disease. *Brain Commun*. 2023;5(6):fcad280.

48. Jack CR Jr, Bennett DA, Blennow K, *et al*. NIA-AA Research Framework: Toward a biological definition of Alzheimer's disease. *Alzheimers Dement*. 2018;14(4):535-562.

49. Albert MS, DeKosky ST, Dickson D, *et al*. The diagnosis of mild cognitive impairment due to Alzheimer's disease: Recommendations from the National Institute on Aging-Alzheimer's Association workgroups on diagnostic guidelines for Alzheimer's disease. *Alzheimers Dement*. 2011;7(3):270-279.

50. McKhann GM, Knopman DS, Chertkow H, *et al*. The diagnosis of dementia due to Alzheimer's disease: Recommendations from the National Institute on Aging-Alzheimer's Association workgroups on diagnostic guidelines for Alzheimer's disease. *Alzheimers Dement*. 2011;7(3):263-269.

51. Villeneuve S, Rabinovici GD, Cohn-Sheehy BI, *et al*. Existing Pittsburgh Compound-B positron emission tomography thresholds are too high: Statistical and pathological evaluation. *Brain*. 2015;138(Pt 7):2020-2033.

52. Rosen HJ, Gorno-Tempini ML, Goldman WP, *et al*. Patterns of brain atrophy in frontotemporal dementia and semantic dementia. *Neurology*. 2002;58(2):198-208.

53. Mueller SG, Laxer KD, Barakos J, Cheong I, Garcia P, Weiner MW. Widespread neocortical abnormalities in temporal lobe epilepsy with and without mesial sclerosis. *Neuroimage*. 2009;46(2):353-359.

54. Iglesias JE, Van Leemput K, Bhatt P, *et al*. Bayesian segmentation of brainstem structures in MRI. *Neuroimage*. 2015;113:184-195.

55. Xu L, Groth KM, Pearlson G, Schretlen DJ, Calhoun VD. Source-based morphometry: The use of independent component analysis to identify gray matter differences with application to schizophrenia. *Hum Brain Mapp*. 2008;30(3):711-724.

56. Wickham H. *ggplot2: Elegant graphics for data analysis*. Springer; 2016.

57. Su Y, Blazey TM, Owen CJ, *et al*. Quantitative amyloid imaging in autosomal dominant Alzheimer's disease: Results from the DIAN Study Group. *PLoS One*. 2016;11(3):e0152082.

58. Klunk WE, Price JC, Mathis CA, *et al*. Amyloid deposition begins in the striatum of presenilin-1 mutation carriers from two unrelated pedigrees. *J Neurosci*. 2007;27(23):6174-6184.

59. Knight WD, Okello AA, Ryan NS, *et al*. Carbon-11-Pittsburgh Compound B positron emission tomography imaging of amyloid deposition in presenilin 1 mutation carriers. *Brain*. 2011;134(Pt 1):293-300.

60. Koivunen J, Verkkoniemi A, Aalto S, *et al*. PET amyloid ligand [11C]PIB uptake shows predominantly striatal increase in variant Alzheimer's disease. *Brain*. 2008;131(Pt 7):1845-1853.

61. Remes AM, Laru L, Tuominen H, *et al*. Carbon 11-labeled Pittsburgh Compound B positron emission tomographic amyloid imaging in patients with APP locus duplication. *Arch Neurol*. 2008;65(4):540-544.

62. Villemagne VL, Ataka S, Mizuno T, *et al*. High striatal amyloid beta-peptide deposition across different autosomal Alzheimer disease mutation types. *Arch Neurol*. 2009;66(12):1537-1544.

63. Scholl M, Wall A, Thordardottir S, *et al*. Low PiB PET retention in presence of pathologic CSF biomarkers in Arctic APP mutation carriers. *Neurology*. 2012;79(3):229-236.

64. Koscik RL, Betthauser TJ, Jonaitis EM, *et al*. Amyloid duration is associated with preclinical cognitive decline and tau PET. *Alzheimers Dement (Amst)*. 2020;12(1):e12007.

65. Schindler SE, Li Y, Buckles VD, *et al*. Predicting symptom onset in sporadic Alzheimer disease with amyloid PET. *Neurology*. 2021;97(18):e1823-e1834.

66. Benzinger TLS, Blazey T, Jack CR Jr, *et al*. Regional variability of imaging biomarkers in autosomal dominant Alzheimer's disease. *Proc Natl Acad Sci U S A*. 2013;110(47):E4502-E4509.

67. Cohen AD, McDade E, Christian B, *et al*. Early striatal amyloid deposition distinguishes Down syndrome and autosomal dominant Alzheimer's disease from late-onset amyloid deposition. *Alzheimers Dement*. 2018;14(6):743-750.

68. Hanseeuw BJ, Lopera F, Sperling RA, *et al*. Striatal amyloid is associated with tauopathy and memory decline in familial Alzheimer's disease. *Alzheimers Res Ther*. 2019;11(1):17.

69. Beach TG, Sue LI, Walker DG, *et al*. Striatal amyloid plaque density predicts Braak neurofibrillary stage and clinicopathological Alzheimer's disease: Implications for amyloid imaging. *J Alzheimers Dis*. 2012;28(4):869-876.

70. Yau WYW, Tudorascu DL, McDade EM, *et al*. Longitudinal assessment of neuroimaging and clinical markers in autosomal dominant Alzheimer's disease: A prospective cohort study. *Lancet Neurol*. 2015;14(8):804-813.

71. Schöll M, Almkvist O, Axelman K, *et al*. Glucose metabolism and PIB binding in carriers of a His163Tyr presenilin 1 mutation. *Neurobiol Aging*. 2011;32(8):1388-1399.

72. Hanseeuw BJ, Betensky RA, Mormino EC, *et al*. PET staging of amyloidosis using striatum. *Alzheimers Dement*. 2018;14(10):1281-1292.

73. Grothe MJ, Barthel H, Sepulcre J, *et al*. *In vivo* staging of regional amyloid deposition. *Neurology*. 2017;89(20):2031-2038.

74. Harper L, Bouwman F, Burton EJ, *et al*. Patterns of atrophy in pathologically confirmed dementias: A voxelwise analysis. *J Neurol Neurosurg Psychiatry*. 2017;88(11):908-916.

75. Shinohara M, Fujioka S, Murray ME, *et al*. Regional distribution of synaptic markers and APP correlate with distinct clinicopathological features in sporadic and familial Alzheimer's disease. *Brain*. 2014;137(Pt 5):1533-1549.

76. Johnson KA, Gregas M, Becker JA, *et al*. Imaging of amyloid burden and distribution in cerebral amyloid angiopathy. *Ann Neurol*. 2007;62(3):229-234.

77. Greenberg SM, Grabowski T, Gurol ME, *et al*. Detection of isolated cerebrovascular beta-amyloid with Pittsburgh Compound B. *Ann Neurol*. 2008;64(5):587-591.

78. Mann DMA, Davidson YS, Robinson AC, *et al*. Patterns and severity of vascular amyloid in Alzheimer's disease associated with duplications and missense mutations in APP gene, Down syndrome and sporadic Alzheimer's disease. *Acta Neuropathol*. 2018; 136(4):569-587.

79. Mann DM, Pickering-Brown SM, Takeuchi A, Iwatsubo T; Members of the Familial Alzheimer's Disease Pathology Study Group. Amyloid angiopathy and variability in amyloid beta deposition is determined by mutation position in presenilin-1-linked Alzheimer's disease. *Am J Pathol*. 2001;158(6):2165-2175.

80. Stankoff B, Freeman L, Aigrot MS, *et al*. Imaging central nervous system myelin by positron emission tomography in multiple sclerosis using [methyl-11C]-2-(4′-methylaminophenyl)-6-hydroxybenzothiazole. *Ann Neurol*. 2011;69(4):673-680.

81. Glodzik L, Rusinek H, Li J, *et al*. Reduced retention of Pittsburgh Compound B in white matter lesions. *Eur J Nucl Med Mol Imaging*. 2015;42(1):97-102.

82. Goodheart AE, Tamburo E, Minhas D, *et al*. Reduced binding of Pittsburgh Compound-B in areas of white matter hyperintensities. *NeuroImage Clin*. 2015;9:479-483.

83. Ryan NS, Biessels GJ, Kim L, *et al*. Genetic determinants of white matter hyperintensities and amyloid angiopathy in familial Alzheimer's disease. *Neurobiol Aging*. 2015;36(12):3140-3151.

84. Lee S, Viqar F, Zimmerman ME, *et al*. White matter hyperintensities are a core feature of Alzheimer's disease: Evidence from the dominantly inherited Alzheimer network. *Ann Neurol*. 2016; 79(6):929-939.

85. Abrahamson EE, Kofler JK, Becker CR, *et al*. 11C-PiB PET can underestimate brain amyloid-β burden when cotton wool plaques are numerous. *Brain*. 2022;145(6):2161-2176.

86. Ni R, Gillberg PG, Bogdanovic N, *et al*. Amyloid tracers binding sites in autosomal dominant and sporadic Alzheimer's disease. *Alzheimers Dement*. 2017;13(4):419-430.

87. Scheuner D, Eckman C, Jensen M, *et al*. Secreted amyloid betaprotein similar to that in the senile plaques of Alzheimer's disease is increased *in vivo* by the presenilin 1 and 2 and APP mutations linked to familial Alzheimer's disease. *Nat Med*. 1996;2(8): 864-870.

88. Mawuenyega KG, Sigurdson W, Ovod V, *et al*. Decreased clearance of CNS β-amyloid in Alzheimer's disease. *Science*. 2010; 330(6012):1774-1774.

89. Potter R, Patterson BW, Elbert DL, *et al*. Increased *in vivo* amyloid-β42 production, exchange, and loss in presenilin mutation carriers. *Sci Transl Med*. 2013;5(189):189ra77.

90. Pagnon de la Vega M, Giedraitis V, Michno W, *et al*. The Uppsala APP deletion causes early onset autosomal dominant Alzheimer's disease by altering APP processing and increasing amyloid β fibril formation. *Sci Transl Med*. 2021;13(606):eabc6184.

91. Chhatwal JP, Schultz SA, McDade E, *et al*. Variant-dependent heterogeneity in amyloid β burden in autosomal dominant Alzheimer's disease: Cross-sectional and longitudinal analyses of an observational study. *Lancet Neurol*. 2022;21(2):140-152.

92. Shepherd C, McCann H, Halliday GM. Variations in the neuropathology of familial Alzheimer's disease. *Acta Neuropathol*. 2009;118(1):37-52.

93. Maarouf CL, Daugs ID, Spina S, *et al*. Histopathological and molecular heterogeneity among individuals with dementia associated with Presenilin mutations. *Mol Neurodegener*. 2008;3:20.

94. Sun L, Zhou R, Yang G, Shi Y. Analysis of 138 pathogenic mutations in presenilin-1 on the in vitro production of Aβ42 and Aβ40 peptides by γ-secretase. *Proc Natl Acad Sci U S A*. 2017;114(4): E476-E485.

95. Liu L, Lauro BM, He A, *et al*. Identification of the Aβ37/42 peptide ratio in CSF as an improved Aβ biomarker for Alzheimer's disease. *Alzheimers Dement*. 2023;19(1):79-96.

96. Gómez-Isla T, Growdon WB, McNamara MJ, *et al*. The impact of different presenilin 1 andpresenilin 2 mutations on amyloid deposition, neurofibrillary changes and neuronal loss in the familial Alzheimer's disease brain: Evidence for other phenotypemodifying factors. *Brain*. 1999;122(Pt 9):1709-1719.

97. Martikainen P, Pikkarainen M, Pöntynen K, *et al*. Brain pathology in three subjects from the same pedigree with presenilin-1 (PSEN1) P264L mutation. *Neuropathol Appl Neurobiol*. 2010;36(1):41-54.

98. Fleisher AS, Chen K, Quiroz YT, *et al*. Florbetapir PET analysis of amyloid-β deposition in the presenilin 1 E280A autosomal dominant Alzheimer's disease kindred: A cross-sectional study. *Lancet Neurol*. 2012;11(12):1057-1065.

99. Dermaut B, Kumar-Singh S, Engelborghs S, *et al*. A novel presenilin 1 mutation associated with pick's disease but not beta-amyloid plaques. *Ann Neurol*. 2004;55(5):617-626.

100. Shi Z, Wang Y, Liu S, *et al*. Clinical and neuroimaging characterization of Chinese dementia patients with PSEN1 and PSEN2 mutations. *Dement Geriatr Cogn Disord*. 2015;39(1–2):32-40.

101. Theuns J, Marjaux E, Vandenbulcke M, *et al*. Alzheimer dementia caused by a novel mutation located in the APP C-terminal intracytosolic fragment. *Hum Mutat*. 2006;27(9):888-896.

102. Lee EC, Kang JM, Seo S, *et al*. Association of subcortical structural shapes with tau, amyloid, and cortical atrophy in early-onset and late-onset Alzheimer's disease. *Front Aging Neurosci*. 2020;12: 563559.

103. Zammit MD, Laymon CM, Tudorascu DL, *et al*. Patterns of glucose hypometabolism in Down syndrome resemble sporadic Alzheimer's disease except for the putamen. *Alzheimers Dement (Amst)*. 2020;12(1):e12138.

104. Thal DR, Rüb U, Orantes M, Braak H. Phases of A beta-deposition in the human brain and its relevance for the development of AD. *Neurology*. 2002;58(12):1791-1800.

105. Braak H, Braak E. Neuropathological stageing of Alzheimer-related changes. *Acta Neuropathol*. 1991;82(4):239-259.

106. Braak H, Alafuzoff I, Arzberger T, Kretzschmar H, Del Tredici K. Staging of Alzheimer disease-associated neurofibrillary pathology using paraffin sections and immunocytochemistry. *Acta Neuropathol*. 2006;112(4):389-404.

107. Braak H, Thal DR, Ghebremedhin E, Del Tredici K. Stages of the pathologic process in Alzheimer disease: Age categories from 1 to 100 years. *J Neuropathol Exp Neurol*. 2011;70(11):960-969.

108. Taddei K, Kwok JB, Kril JJ, *et al*. Two novel presenilin-1 mutations (Ser169Leu and Pro436Gln) associated with very early onset Alzheimer's disease. *Neuroreport*. 1998;9(14):3335-3339.

109. Lehmann M, Ghosh PM, Madison C, *et al*. Diverging patterns of amyloid deposition and hypometabolism in clinical variants of probable Alzheimer's disease. *Brain*. 2013;136(Pt 3): 844-858.

110. Laforce R Jr, Tosun D, Ghosh P, *et al*. Parallel ICA of FDG-PET and PiB-PET in three conditions with underlying Alzheimer's pathology. *NeuroImage Clin*. 2014;4:508-516.

111. Vanhoutte M, Semah F, Rollin Sillaire A, *et al*. ¹⁸F-FDG PET hypometabolism patterns reflect clinical heterogeneity in sporadic forms of early-onset Alzheimer's disease. *Neurobiol Aging*. 2017;59:184-196.

112. Lippa CF, Saunders AM, Smith TW, *et al*. Familial and sporadic Alzheimer's disease: Neuropathology cannot exclude a final common pathway. *Neurology*. 1996;46(2):406-412.

113. Ishii K, Lippa C, Tomiyama T, *et al*. Distinguishable effects of presenilin-1 and APP717 mutations on amyloid plaque deposition. *Neurobiol Aging*. 2001;22(3):367-376.

114. Balasa M, Vidal-Piñeiro D, Lladó A, *et al*. PSEN1 mutation carriers present lower cerebrospinal fluid amyoid-β42 levels than sporadic early-onset Alzheimer's disease patients but no differences in neuronal injury biomarkers. *J Alzheimers Dis JAD*. 2012;30(3):605-616.